HUNGARIAN AGRICULTURAL ENGINEERING
No 41/2022 17-23
Published online: http://hae-journals.org/
HU ISSN 0864-7410 (Print)
HU ISSN 2415-9751(Online)
DOI: 10.17676/HAE.2022.41.17
Received: 20.04.2022 - Accepted: 15.05.2022

PERIODICAL
OF THE COMMITTEE OF AGRICULTURAL AND BIOSYSTEM ENGINEERING OF THE HUNGARIAN ACADEMY OF SCIENCES
and
HUNGARIAN UNIVERSITY OF AGRICULTURE AND LIFE SCIENCES INSTITUTE OF TECHNOLOGY

HUNGARIAN UNIVERSITY OF AGRICULTURE AND LIFE SCIENCES
Institute of Technology

MODELING THE EFFECT OF WHEEL TRAVELING ON THE SOIL SURFACE ON THE LOAD OF BURIED STRUCTURE

Author(s):
I. Keppler

Affiliation:
Institute of Technology - Hungarian University of Agriculture and Life Sciences, 2100 Gödöllő, Páter Károly u. 1., Hungary;

Email address:
keppler.istvan@uni-mate.hu

Abstract: As a result of the technical development of agriculture, machines with very high axle loads appeared in the fields and on farm roads. As a result, subsurface soil pressure values will also increase, which will ultimately put increased stress on underground pipelines and other structures. In our paper, we show the possibility of modelling the problem using explicit dynamical methods by means of a simple example.

Keywords: discrete element method, soil pressure, underearth pipelines, axle loads, explicit dynamical method

1. Introduction

(Keller and Or 2022) demonstrated that while surface contact stresses remained nearly constant over the course of modern mechanization, subsoil stresses have propagated into deeper soil layers. It can be assumed that this will lead to an increase in the load on the subsurface structures.

Because of the complexity of the structure-soil interaction, buried underearth structures (i.e. pipes) and surrounding soils jointly bear external loads (Bildik and Laman, 2019). The simplified analytical model if the soil pressure considers the soil prism above the subsoil structure (Yu et. al. 2022), and by considering the soil density and "wall" friction the equilibrium of infinitesimal soil slices results a differential equation which has a solution giving the load on a pipe buried in depth H to be

$$\sigma_M = \frac{1 - e^{-\frac{2fK}{B}H}}{2fK}\gamma B$$

where σ_M is the vertical pressure, H is the cover depth, B is the trench width, γ is the unit weight of the backfill, f is the soil-soil friction coefficient and K is the Rankine active soil pressure coefficient. This model is not suitable for the determination of the pressure load arising from the wheel rolling on the surface of this soil-pipe structure.

Several experimental investigations were made for determining the pressure load of buried pipes. Shmulevich et al. (1986) carried out experimental studies and showed that soil pressures have approximately parabolic distribution. Talesnick and Frydman (2018) measured the soil pressure on a 0.8 m-diameter pipe during installation and varied traffic loading.

Several authors have worked on modelling this phenomenon using the finite element method. (Ahmed et al., 2015) evaluated the effect of geogrid on the soil pressure. (Wu et. al. 2021) made sensitivity study regarding the FE model of soil – pipe interaction. (Kang 2019) analysed the effect of imperfect trench installations. The effect of internal friction has been studied by (Whidden 2009). (Zamanian et. al. 2020) considered the influence of hydrostatic pressure on the yield strength and shear dilatancy of the soil.

Analytical solutions of this problem adequate for taking into account even the acceleration of the moving wheel do not exist, this is why our focus has turned towards the application of explicit dynamics modelling method. Instead of soil mechanics relations based on the results of classical continuum mechanics, explicit dynamical methods using the computational power of modern computing tools can provide a more accurate

picture of the load conditions. For modelling the problem, we will use the so-called discrete element modelling method. The discrete element method was developed for rock mechanics in the late 1970s (Cundall and Strack, 1979). The method, which was later developed further, has now become suitable for modelling almost any problem where granular materials interact with their environment or with each other. Such a problem is the effect of soil pressure on underground structures. Using the potential of the new method, it is also possible to model the load variations caused by a moving wheel passing over the pipeline.

2. The discrete element method

For modelling the mechanical behaviour of the granular material, EDEM discrete element software was used. In the discrete element model the simulation evaluates the contact forces according to the "Hertz-Mindlin no slip" contact model: the material and interaction parameters have their effect on the normal- and tangential forces. These forces and moments acting between the interacting soil particles in the form of the following equations [2].

The normal force is calculated using

$$F_n = \frac{4}{3}E_0\delta^{\frac{3}{2}}\sqrt{R_0} - 2\sqrt{\frac{5}{6}}\frac{\ln C_r}{\sqrt{\ln^2 C_r+\pi^2}}\sqrt{2E_0}\sqrt[4]{R_0\delta}\sqrt{m_0}v_{\mathrm{nrel}},$$

where $\frac{1}{E_0} = \frac{1-\nu_1^2}{E_1} + \frac{1-\nu_2^2}{E_2}$ is the equivalent Young modulus of the two interacting soil particles, δ is the overlap between these two soil particles. This normal overlap represents the normal deformation of a particle. The normal overlap δ between two particles i and j at positions x_i and x_j (where x is the distance measured on the line connecting the centres of the two overlapping particles) with radii R_i and R_j is defined as: $\delta = R_i + R_j - (x_j - x_i)$. $R_0 = \frac{R_1R_2}{R_1+R_2}$ is the equivalent radius, $\mathrm{m}_0 = \frac{\mathrm{m}_1\mathrm{m}_2}{\mathrm{m}_1+\mathrm{m}_2}$ is the equivalent mass and v_{nrel} is the normal component of the relative velocity of the soil particles.

The tangential force can be calculated as

$$F_t = -8G_0\sqrt{R_0\delta}\delta_t - 2\sqrt{\frac{5}{6}}\frac{\ln C_r}{\sqrt{\ln^2 C_r+\pi^2}}\sqrt{2G_0}\sqrt[4]{R_0\delta}\sqrt{m_0}v_{\mathrm{trel}},$$

where $\frac{1}{G_0} = \frac{2-\nu_1}{G_1} + \frac{2-\nu_2}{G_2}$ is the equivalent shear modulus of the two interacting soil particles, δ_t is the tangential overlap between the two particles and v_{trel} is the tangential component of the relative velocity of the soil particles. The tangential overlap is the tangential displacement of the contact point up to the point at which the contact ends or the particle begins to roll or slip. The tangential overlap represents the tangential deformation of a particle. The tangential force is limited by Coulomb friction $\mu_s F_n$, where μ_s is the coefficient of static friction.

The moment from rolling friction is $M_r = -\mu_r F_N R_i \omega_i$, where R_i is the distance of the contact point from the centre of the i-th soil particles and ω_i is the unit angular velocity vector, which is a dimensionless quantity representing only the direction of rotation of the i-th soil particle. μ_r is the coefficient of rolling friction. The tangential force also has moment on the particle: $M_t = F_t R_i$.

According to (Potyondy and Cundall, 2004), from $t > t_{\mathrm{bond}}$ (from the time, when bonding is "turned on") at contact points and at points which are closer to each other than a pre-defined distance (called bonded disk radius) particles are glued to each other by bonding bridges. Bonds of finite stiffness can exist at contacts, and these bonds carry load and can break. An applied macroscopic load is carried by the grain and "glue" skeleton in the form of force chains that propagate from one grain to the next across grain contacts, some of which may be filled with "glue". The forces arising in these bonding bridges can be calculated by taking into account their deformation and their material properties.

The bonding forces/moments acting on the particles are set to initial value zero, and are adjusted incrementally every time step:

$$\delta F_n = -v_n S_n A \delta t,$$

$$\delta F_t = -v_t S_t A \delta t,$$

$$\delta M_n = -\omega_n S_t J \delta t,$$

$$\delta M_t = -\omega_t S_n \frac{J}{2} \delta t,$$

where $A = R_B^2\pi$, $J = \frac{1}{2}R_B^4\pi$. R_B is the radius of the glue, $S_{n,t}$ are the normal and shear stiffness per unit area, $\delta t$is the timestep, $v_{n,t}$ are the normal and tangential velocities of the particles and $\omega_{n,t}$ are the normal and tangential components of the angular velocity vector.

The bond is broken when the normal or tangential stress exceeds some predefined value (the strength of the bonding bridges):

$$\sigma < -\frac{F_n}{A} + \frac{2M_t}{J}R_{Bmax}\,,$$

$$\tau < -\frac{F_t}{A} + \frac{M_t}{J}R_{Bmax}.$$

These bonding forces/torques are in addition to the standard Hertz-Mindlin forces.

During the simulations, the linear- and angular momentum theorem is used to write the equation of motion for all the individual particles resulting multiple number of differential equations to be solved in a sufficiently large number of time steps. The used time step has a great impact on the stability of the numerical model. We selected for the simulation 25% of the Rayleigh-type time step:

$$\delta t = 0{,}25T_R = 0{,}25 \cdot (0.1631\nu + 0{,}8766)^{-1}\pi R\left(\frac{\rho_p}{G_p}\right)^{\frac{1}{2}}.$$

It is important to consider that the quality of the obtainable solution could sensitively depend on the value of this time step used during the simulations. The same time step must be used during the calibration process of the discrete element model and during the simulations.

3. Materials and Methods

Among the possible explicit dynamic modelling procedures, the discrete element method was used to study the phenomenon. A very important advantage of the modelling procedure we have chosen is that it can also track the wheel separation under load conditions during wheel motion. This is not possible at all with analytical methods and is rather difficult with solutions based on the finite element method.

3.1. The discrete element model

The discrete element model of the soil-wheel-pipe structure can be seen on (Figure 1). The model consists of a *D*=420mm finned rigid wheel, approximately 45000soil particles and a radius *R*=100mm half pipe created from 10 segments to make it possible to determine the soil pressure distribution on its surface. The soil depth under the wheel was approximately 2000mm, which is quite small, but our goal was only to demonstrate the possibilities of DEM modelling.

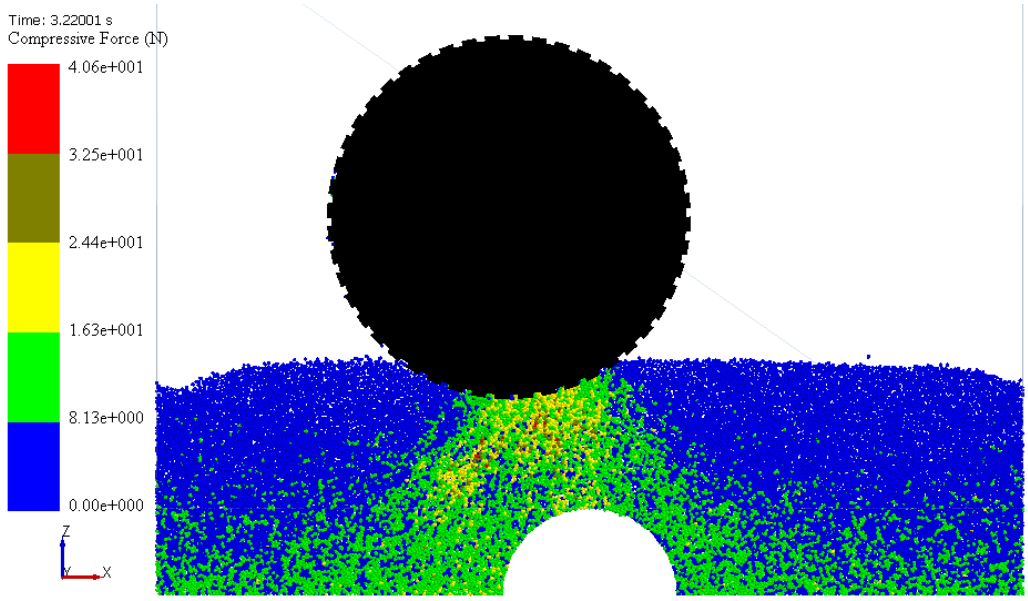

Figure 1. DEM model of the soil – wheel – pipe structure, particle-particle compressive force is shown

For the discrete element model of soil, we used the following calibrated (based on the modelling of the standard shear test) data from (Keppler et. al. 2015):

- Poisson's ratio $\nu_p = 0.25$, $\nu_t = 0.3$
- Shear modulus $G_p = 10^7$Pa, $G_t = 8 \cdot 10^9$ Pa,
- Density $\rho_p = 3000$ kgm^{-3}, $\rho_t = 7500$ kgm^{-3},
- Coefficient of restitution: $C_{r,p-p} = C_{r,t-p} = 0.5$,
- Coefficient of static friction $\mu_{p-p} = 0.9$, $\mu_{p-t} = 0.3$,
- Coefficient of rolling friction $\mu_{r,p-p} = 0.01$, $\mu_{r,p-t} = 0.01$.

And for the bonded soil model we used:

- Normal stiffness: $S_n = 10^9$ Nm^{-3},
- Shear stiffness $S_t = 10^9$ Nm^{-3},
- Critical normal stress $\sigma_{max} = 1.5 \cdot 10^6$ Pa,
- Critical shear test $\tau_{max} = 8 \cdot 10^5$ Pa,
- Bonded disk radius $R_B = 0.006$m.

Subscript *p* means particle, *t* means other structural elements in the model. The bulk material particles were created as a clump of two spheres having 2 mm radiuses and 1.5 mm distance between the two spherical surfaces resulting one clumped particle. The whole geometrical configuration involved periodic boundaries in *x* and *y* directions (see Figure 1.). This means quite similar "infinite" extent of the model to the direction perpendicular (*y*) direction of the figure and behaves like the plain strain model in classical continuum modelling. The kinematical parameters of the wheel were $v_0 = 0$ initial velocity and $a = 0.47 \frac{\text{m}}{\text{s}^2}$ constant acceleration. This resulted the rolling of the wheel above the pipe without sliding. We used 25% of the Raileigh time step during the DEM modelling calculations.

3.2. Data analysis

After the running of the simulations, we analysed the pressure distribution arising on the surface of the pipe segments. On Figure 2. you see the pressure overload of the topmost horizontal segment of the pipe caused by the rolling wheel.

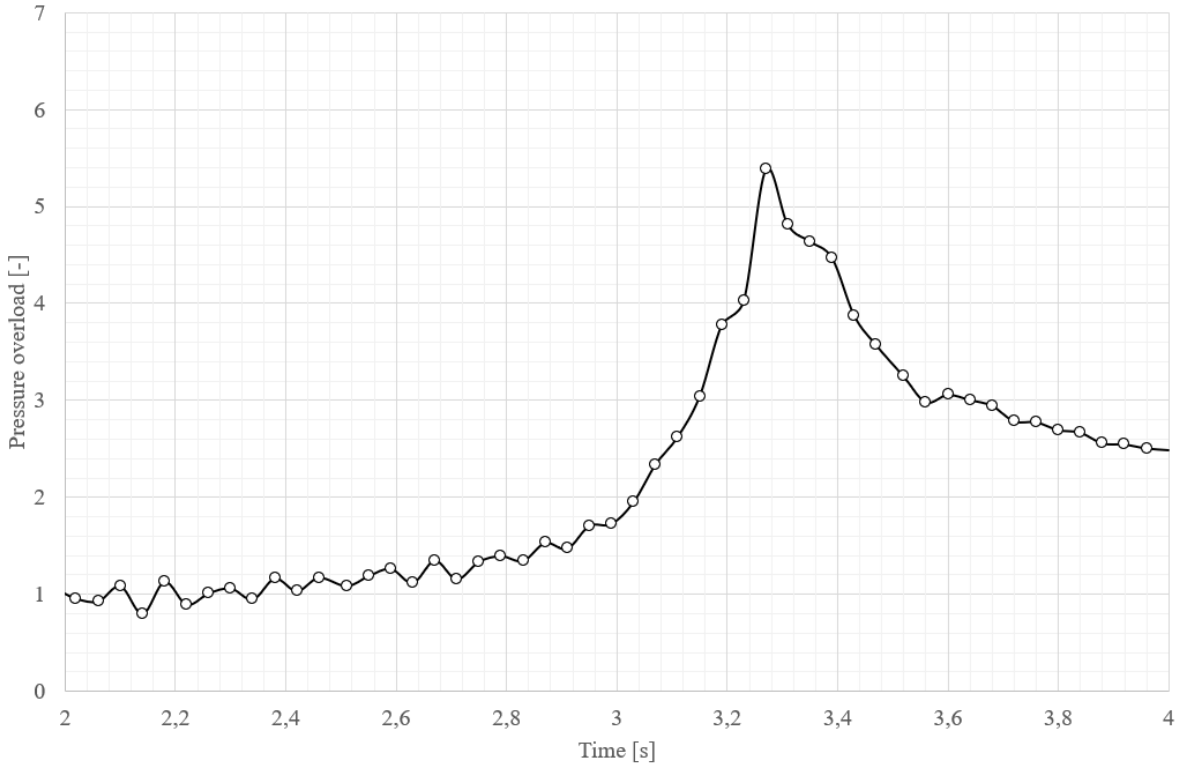

Figure 2. Pressure overload caused by the wheel rolling over the pipe

The pressure overload was calculated as the pressure arising from the soil resting above the pipe divided by the pressure caused by the rolling wheel. Of course, this value highly depends on the axle load (in our case it was 500N), but the goal of this article is to demonstrate the capabilities of the DEM modelling, so the concrete value is not so important for us. The cause of the pressure overload is the change in the force distribution between the soil particles (Figure 3.).

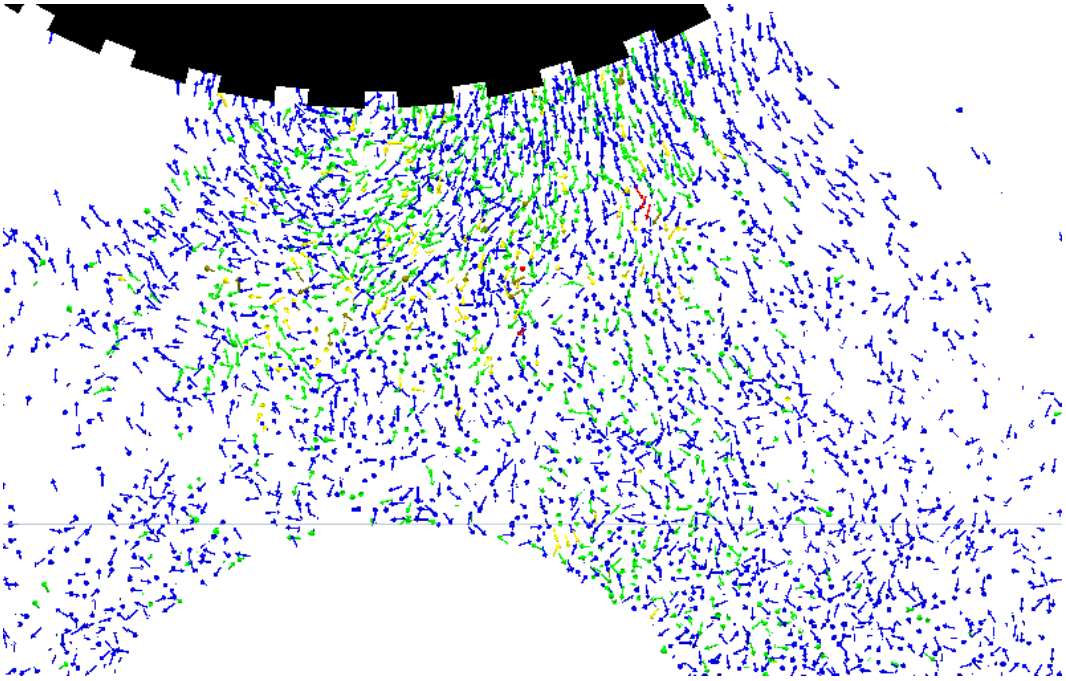

Figure 3. Particle force distribution vector field above the pipe segment

4. Results

Having all these data for all the pipe segments, we created the pipe wall overload diagram, by calculating the maximal pressure overload for all pipe segments. It is worth to note, that by using this method we have the chance to find the maximal overload values for all the separate pipe segments, although these quantities appear in different positions of the wheel for each segment.

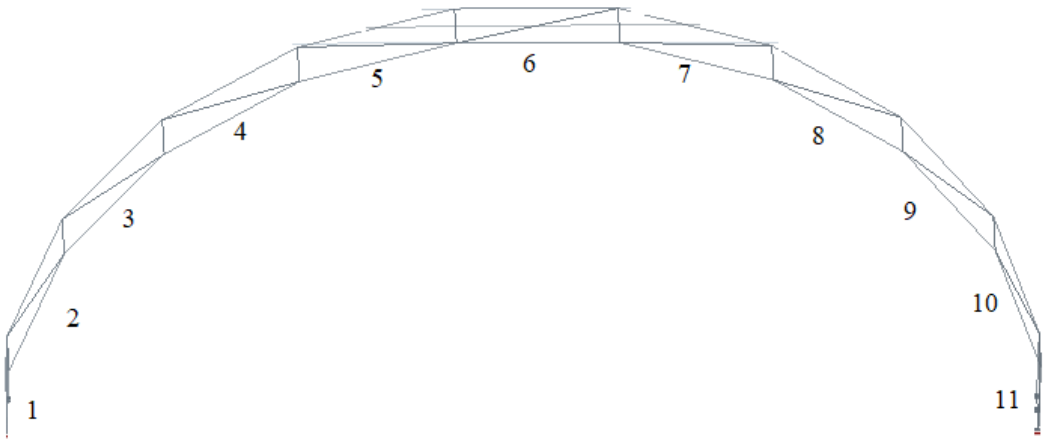

Figure 4. Pipe segments for pressure distribution data

Figure 5 shows the pressure overload values on all the pipe segments listen on Figure 4.

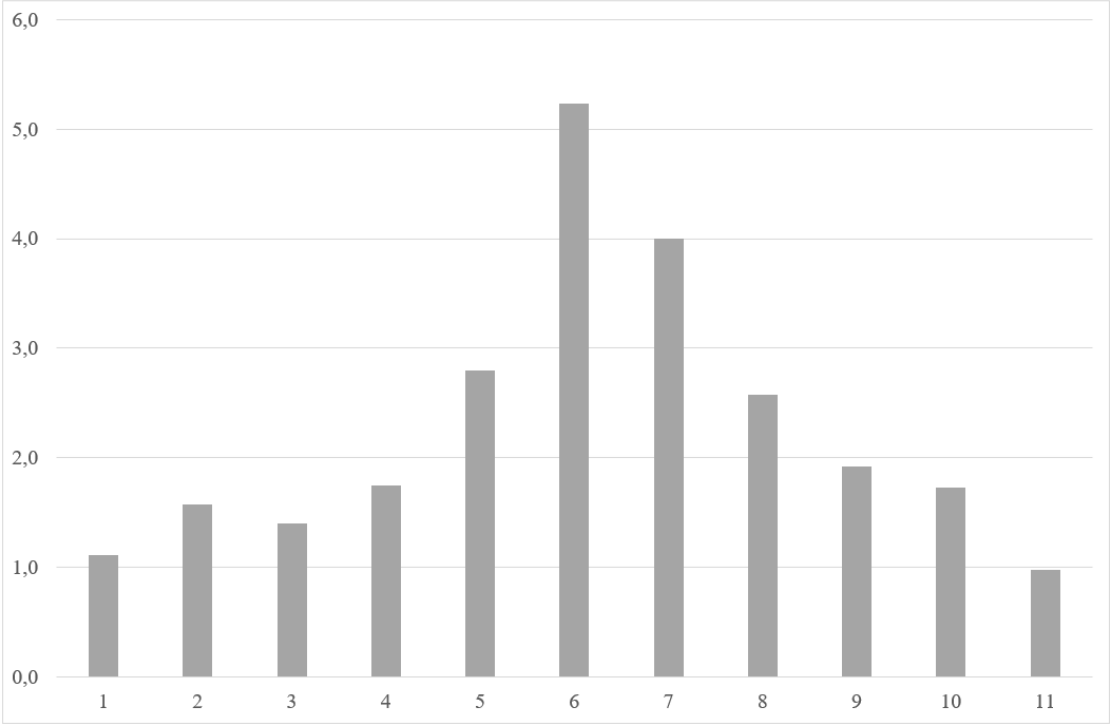

Figure 5. Pressure overload of the different pipe segments.

The results of the numerical simulation show that the highest overload is expected at the top of the pipe. This shows a good match between the results of the exercise and the "expected" physical behaviour as Zhou et al. (2011) and Li (2017) who studied the 0.61 diameter and 0.1 m-diameter pipes, respectively, and both depicted that the soil pressure is the largest at the pipe crown and has roughly parabola distribution.

5. Conclusions

What we found was that the side of the tube towards which the wheel was approaching was subjected to much higher loads than the other side, and the highest overload is expected at the top of the pipe.

The method presented here provides a more detailed picture of the mechanical processes occurring in the granular assemblies and about their interaction with the structures under investigation than the classical analytical solutions. Our primary objective in this article was to investigate the applicability of the DEM-based method. It follows that the results obtained can only be applied in practice after further experimental and numerical analysis. However, we have been able to demonstrate that the application of DEM-based methods can be realistic in the field of the present study. Of course, the applicability of the specific numerical results requires a number of further tests.

Acknowledgements

The research was funded by the project "Development of mobile mechatronic industrial applications using laser and structural stress measurement technologies" and "KFI 16-1-2017-0216".

References

[1] Keller Thomas, Or Dani (2022). Farm vehicles approaching weights of sauropods exceed safe mechanical limits for soil functioning, Proceedings of the National Academy of Sciences, 2022 Vol. 119 No. 21 e2117699119

[2] Bildik, S., Laman, M. (2019). Experimental investigation of soil-structure pipe interaction. KSCE J. Civ. Eng. 23 (9), 3753–3763.

[3] **Jin-Hong Yu, He-Gao Wu, Chang-Zheng Shi, Zhu Ma, Wen-Tao Xu** (2022). Behavior and innovative design model on soil pressure at the top of large-diameter buried steel pipes, Soils and Foundations 62 (2022) 101153.

[4] **Shmulevich, I., Galili, N., Foux, A. (**1986). Soil stress distribution around buried pipes. J. Transp. Eng. 112 (5), 481–494

[5] **Talesnick, M.L., Frydman, S.** (2018). Soil pressure and pipe deformation measurements for characterizing flexible pipe–soil systems under shallow cover. J. Pipeline Syst. Eng. Pract. 9 (1).

[6] **Ahmed, M.R., Tran, V.D.H., Meguid, M.A. (**2015). On the role of geogrid reinforcement in reducing earth pressure on buried pipes: experimental and numerical investigations. Soils Found. 55 (3), 588–599

[7] **Wu, H.G., Yu, J.H., Shi, C.Z., Ma, Z.** (2021). Pipe-soil interaction and sensitivity study of large-diameter buried steel pipes. KSCE J. Civ. Eng. 1 (12), 793–804.

[8] **Cundall, P.A. and Strack,** O.D.L. (1979). A discrete numerical model for granular assemblies, Geotechnique, Vol. 29 No. 1, pp. 47-65.

[9] **D.O. Potyondy, P.A. Cundall** (2004). A bonded-particle model for rock, International Journal of Rock Mechanics & Mining Sciences 41 1329–1364

[10] **Keppler I., Hudoba Z., Oldal I., Csatar A., Fenyvesi L.** (2015). Discrete element modeling of vibrating tillage tools, Engineering Computations, Volume 32, Issue 2, Pages 308-328.

[11] **Zhou, Z.F., Ling, J.M., Liang, B.** (2011). Analysis of earth pressure on oil pipe. Journal of Chongqing Jiaotong University. Natural Sci. 30 (4), 794–797.

[12] **Li, Y.G.** (2017). Experimental study on earth pressure distribution around buried pipeline. Henan University of Technology (in Chinese), Zhengzhou.

[13] **Kang, J.** (2019). Finite element analysis for deeply buried concrete pipes in proposed imperfect trench installations with expanded polystyrene (EPS) foams. Eng. Struct. 189, 286–295.

[14] **Whidden, W.R.** (2009). Buried flexible steel pipe: design and structural analysis. ASCE Manuals and Reports on Engineering Practice No 119, Reston, Virginia, USA.

[15] **Zamanian, S., Hur, J., Shafieezadeh, A.** (2020). A high-fidelity computational investigation of buried concrete sewer pipes exposed to truckloads and corrosion deterioration. Eng. Struct. 221